High Energy Density Physics 26 (2018) 26–37

Contents lists available at ScienceDirect

High Energy Density Physics

journal homepage: www.elsevier.com/locate/hedp

An automated design process for short pulse laser driven opacity experiments

M.E. Martin[a,b,*], R.A. London[a], S. Goluoglu[b], H.D. Whitley[a]

[a] Lawrence Livermore National Laboratory, P.O. Box 808, Livermore, California 94550, United States
[b] Nuclear Engineering Program, Department of Materials Science and Engineering, University of Florida, PO Box 116400, Gainesville, Florida 32611, United States

ARTICLE INFO

Keywords:
Opacity
Emission
Design
Optimization
Stellar
Laser

ABSTRACT

Stellar-relevant conditions can be reached by heating a buried layer target with a short pulse laser. Previous design studies of iron buried layer targets found that plasma conditions are dominantly controlled by the laser energy while the accuracy of the inferred opacity is limited by tamper emission and optical depth effects. We developed a process to simultaneously optimize laser and target parameters to meet a variety of design goals. We explored two sets of design cases: a set focused on conditions relevant to the upper radiative zone of the sun (electron temperatures of 200 to 400 eV and densities greater than 1/10 of solid density) and a set focused on reaching temperatures consistent with deep within the radiative zone of the sun (500 to 1000 eV) at a fixed density. We found optimized designs for iron targets and determined that the appropriate dopant, for inferring plasma conditions, depends on the goal temperature: magnesium for up to 300 eV, aluminum for 300 to 500 eV, and sulfur for 500 to 1000 eV. The optimal laser energy and buried layer thickness increase with goal temperature. The accuracy of the inferred opacity is limited to between 11% and 31%, depending on the design. Overall, short pulse laser heated iron experiments reaching stellar-relevant conditions have been designed with consideration of minimizing tamper emission and optical depth effects while meeting plasma condition and x-ray emission goals.

1. Introduction

Short pulse lasers have been used to heat materials to hundreds of eVs at near solid densities [1–12]. X-ray emission measurements, at such stellar-relevant conditions, may provide insight into existing disagreements between solar models and observations [13–21] by testing the validity of theoretical opacity models. In addition, short pulse heated emission measurements would complement previous absorption measurements that used long pulse lasers [22–28] and pulsed power machines [29–32]. Laser parameters and target dimensions can be optimized to design short pulse experiments that reach a range of stellar-relevant conditions.

We previously examined the effects of short pulse laser irradiance and target dimensions on plasma conditions, x-ray emission, and the opacity inference for iron buried layers. We found that peak plasma temperature and x-ray emission increase with laser energy and the opacity inference is limited by tamper emission and optical depth effects [33]. Our earlier work resulted in an example design that mitigated optical depth and tamper emission effects, but the design was not selected using a formal optimization process. In this paper, we expand upon our work by implementing an automated process to systemically explore a broad range of laser and target parameters and find optimized designs therein. This allows us to determine globally optimized designs for specific goals, such as plasma temperature and density. We used the process to find optimized designs of buried iron sulfide (FeS_2) targets. The choice of iron sulfide is motivated by experiments at Atomic Weapons Establishment's Orion Laser Facility, which were originally proposed to use 0.3 μm iron sulfide sandwiched between two 3 μm layers of parylene-N.[1] The experiments were planned to use a 0.53 μm wavelength laser beam with a pulse length of 0.5 ps [34], focused to 20 – 50 μm diameters [8], and laser energies up to 100 J [34]. We explored two sets of design cases using the automated process. The first set focused on the range of plasma conditions relevant to the upper radiative zone of the sun: $T = 200$ eV, $T = 300$ eV, and $T = 400$ eV, each with $\rho > 1/10$ of solid density. The second set focused on reaching higher plasma temperatures, relevant to deep within the radiative zone of the sun, at a fixed density: $T = 500$ eV, $T = 750$ eV, and $T = 1000$ eV, each with $\rho = 4.2$ g/cm^3. The designs for both sets may be valuable for investigating how iron opacity scales with temperature. In this paper, we discuss the automated design process and its application to these six

* Corresponding author.
E-mail address: memartin@llnl.gov (M.E. Martin).
[1] D. Hoarty, personal communication (2017)

https://doi.org/10.1016/j.hedp.2017.12.001
Received 14 August 2017; Received in revised form 6 December 2017; Accepted 18 December 2017
Available online 21 December 2017

design cases.

In this paper, we use a simulation methodology (Section 2.3) similar to the methodology in our previous work [33]. This methodology assumes 1D geometry, which is most applicable to experiments using a buried microdot target in which the laser focal spot is much larger than the thickness of the buried layer and the microdot diameter. Recent work suggests that for experiments in which the laser focal spot diameter is similar to that of the microdot, the inclusion of radial temperature gradients in analysis is important for fitting measured streaked K-shell spectra [35]. Hoarty et al. concluded that radial temperature gradients may be reduced by either using a smaller microdot or increasing the laser focal spot diameter. We recognize that even though our methodology has been shown to predict peak plasma conditions and reasonable x-ray emission durations [33], it does not include 2D effects which may affect the analysis of experimental data. We have included further discussion of simulation assumptions in Section 2.3 and how they may impact the application of this work in Section 4.

2. Automated design process

We developed an automated design process using the LLNL Uncertainty Quantification Pipeline (UQP) [36–38] to manage and analyze ensembles of HYDRA [39] simulations of the target dynamics. Fig. 1 shows the process steps. We analyze the ensembles using scripts written in Python [40] and Yorick [41]. In the following sections, we describe the opacity inference equation, the general optimization problem addressed in the design process, the HYDRA simulation methodology, the UQP ensemble management, and the post-ensemble analysis process.

2.1. Opacity inference

In a short pulse experiment, the x-ray emission can be used to infer opacity by inverting the solution to the radiation transfer equation:

$$\kappa_\nu = \frac{-ln\left(1 - \frac{I_\nu}{B_\nu(T)}\right)}{\rho\Delta l} \tag{1}$$

where κ_ν is the frequency dependent opacity, I_ν is the measured specific intensity, $B_\nu(T)$ is the Planck function, T is the inferred electron temperature, and $\rho\Delta l$ is the initial areal density of the target. The opacity inference equation Eq. (1) assumes constant local thermodynamic equilibrium (LTE) conditions. A dopant material, that will be ionized to its K-shell, is typically included in the buried layer so that the plasma temperature (T) can be inferred from relative line intensities and the electron density can be inferred from the Stark broadened line widths. The effects of the departure from LTE are typically quantified by comparing LTE and non-LTE models.

2.2. Optimization formulation

We define an ideal design as one in which the simulated inferred opacity (κ_ν) agrees with the opacity supplied to HYDRA (κ_ν^{model}) and meets design constraints at peak temperature. We have defined a general design optimization procedure that minimizes the average relative difference between inferred and model opacity, while satisfying a number of constraints. The average relative difference is

$$\sigma_{\kappa_\nu}^{\text{rel}} = \frac{abs(\kappa_\nu - \kappa_\nu^{model})}{\kappa_\nu^{model}} \tag{2}$$

and the design constraints are summarized in Table 1. The design constraint forms are normalized by the relevant design constraint value, indicated with "*", so that the equations are unitless. In each constraint form, the variable indicated as "peak" refers to the appropriate single value metric at peak temperature to compare with the design constraint value. Our constrained optimization problem can be converted to an unconstrained problem by defining a cost function that includes a penalty function [42,43] for each unsatisfied constraint. We define the cost function as

$$\beta\sigma_{\kappa_\nu}^{\text{rel}} + \Sigma_{i=1}^{m}\phi(\alpha_i, g_i) \tag{3}$$

where β is the relative difference coefficient, $\sigma_{\kappa_\nu}^{\text{rel}}$ is defined in Eq. (2) and $\phi(\alpha_i, g_i)$ are penalty functions with parameters $\{\alpha_i\}$ and constraint functions $\{g_i\}$. We used the following penalty function form in this study:

$$\phi(\alpha_i, g_i) = \begin{cases} 0, & g_i < 0 \\ \alpha_i g_i^2, & g_i \geq 0 \end{cases} \tag{4}$$

where the constraint functions $\{g_i\}$ are the left hand side of the constraint forms in Table 1. We set the constraint functions, penalty parameters, and relative difference coefficient for each design case. We calculate the cost function Eq. (3) for each ensemble simulation then use quantitative optimization techniques (Section 2.4.2) to find the design parameters that yield the minimum cost function.

2.3. HYDRA simulations

We used the HYDRA radiation hydrodynamics code for the target simulations included in each ensemble. Our simulation methodology is

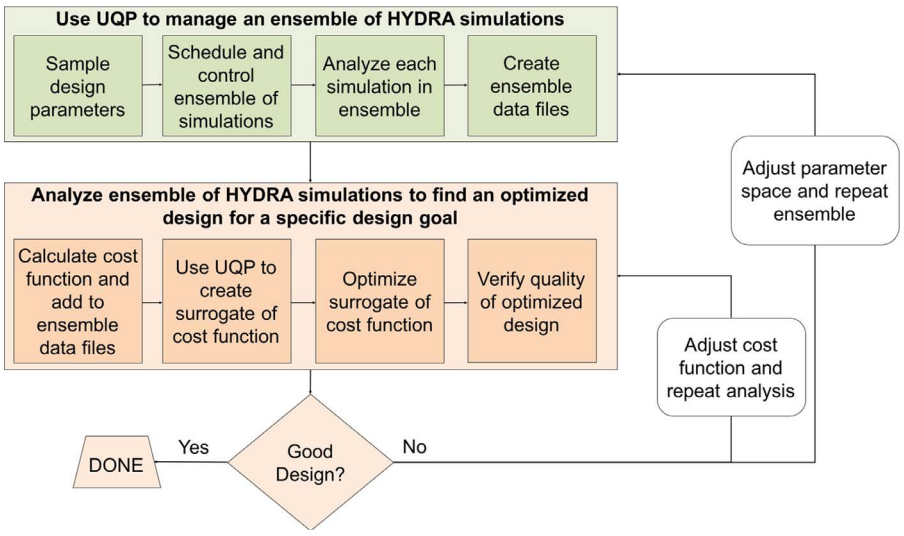

Fig. 1. Flow chart of the automated design process we developed.